International Journal of ChemTech Research
CODEN (USA): IJCRGG ISSN: 0974-4290
Vol.7, No.3, pp 1481-1487, 2014-2015

ICONN 2015 [4th - 6th Feb 2015]
International Conference on Nanoscience and Nanotechnology-2015
SRM University, Chennai, India

Structural, Optical and Magnetic properties of Copper (Cu) doped Tin oxide (SnO_2) nanocrystal

K. Sakthiraj, B.Karthikeyan and K. Balachandrakumar*

Department of Physics, Kamaraj College of Engineering and Technology, Virudhunagar-626001, Tamilnadu, India.

Abstract: Nanocrystal of basic composition $Sn_{1-x}Cu_xO_2$ with x=0.00, 0.02, 0.03 and 0.04 were synthesized by sol-gel route. The samples were characterized using X-ray diffraction (XRD), Fourier transformed infrared spectroscopy (FTIR), UV-Vis spectroscopy, Photoluminescence (PL) spectroscopy and Vibrating sample magnetometer (VSM) measurements. The XRD analysis reveals that the Cu dopants were substituted into rutile SnO_2 nanoparticles without forming any secondary phase. The average particle size of the samples was decreased with increasing Cu concentration. The optical absorption measurements exposed the nanometric size of the materials influences the energy band gap. From the PL spectra, the intense luminescent peak was originated due to the structural defects such as oxygen vacancies. Room temperature M-H curve of pure SnO_2 nanoparticles exhibits ferromagnetic behaviour, while the $Sn_{0.98}Cu_{0.02}O_2$ sample reflects the diamagnetic behaviour. Ultimately, it has been observed that the ferromagnetic property depends on host lattice structural defects rather than impurity phase.
Keywords: Structural, Optical and Magnetic properties, Copper (Cu) doped , Tin oxide (SnO_2) nanocrystal.

Introduction:

Wide band gap oxide based dilute magnetic semiconductors (DMSs) such as SnO_2, ZnO, TiO_2, CeO_2 and In_2O_3 doped with transition metal ions (Mn, Fe, Co, Ni, Cu etc.) have concentrated due to number of unusual electronic and magnetic properties[1-5]. Among these, Tin oxide exhibits notable behavior because of native oxygen vacancy, high carrier density and transparency. This type of oxide semiconductor has particular advantages such as easy integration with semiconductor devices in the field of spintronics, ferromagnetic dilute magnetic semiconductors. Tin oxide materials have many direct applications such as semiconducting gas sensors, solar cell, photo detectors and catalyst for oxidation[6-11]. Ferromagnetic behavior is originated in this oxide semiconductor might be due to introduction of small amount of transition metal (TM) ion, secondary phases and defects rather than ferromagnetic elements. Nanometric size can also influence on the various physical properties of not only the host semiconductor but also the DMS material derived from them. Undoped tin oxide nanoparticles have RTFM while their corresponding bulk sample is diamagnetic[12]. From the magnetic properties of TM doped tin oxide nanostructure, an important understanding has developed that lattice defects can contribute to magnetic signal. Defects can be introduced in metal oxide crystals by doping[13,14] or by varying the oxygen stoichiometry[15], which leads to the modification in the electronic band structure of the material. SnO_2 nanostructures have been prepared by various techniques[16-24]. From this, sol-gel method is an effective

method for creating RTFM in oxide semiconductor. In this work we synthesized $Sn_{1-x}Cu_xO_2$ nanocrystal by a sol-gel method and investigated the structural, optical and magnetic properties of Cu doped SnO_2 powder.

Experimental procedure:

Undoped and Cu doped SnO_2 powders were synthesized by sol-gel technique. The chemicals used in this study were tin (IV) chloride pentahydrate ($SnCl_4.5H_2O$, Sigma Aldrich), ammonium hydroxide (NH_4OH 25%, Sigma Aldrich), Copper sulphate ($CuSO_4$, Sigma Aldrich) and ultra pure water. All reagents used were of analytical grade without further purification.

0.05 M tin (IV) chloride was added to 50 mL of ultra pure water in a round bottom flask and stirring was done for 30 min. A certain amount of ammonia solution (25%) was added into the mixture under a controlled feed rate of 5 drops per min until the pH of the solution became 3 and maintained constant stirring. After 2h of stirring, it formed the white coloured $Sn(OH)_2$ precipitate called sol. The sol was ultrasonically agitated for 15 min and then aged at room temperature for 5 days. The resulting gel was then washed with ethanol and ultra pure water for so many times to remove impurities. The gel was dried at 100ºC for 10 h in air, the obtained powder was ground using mortar and pestle and finally calcinated at 550ºC for 2 h.

For preparing $Sn_{1-x}Cu_xO_2$ nanoparticles, the calculated amount of Copper sulphate ($CuSO_4$) was added to the above sol solution and stirred it for another 1hour. Copper doping ratio was the molar ratio of Cu/(Cu+Sn), namely x. Similar experimental procedure was applied to obtain Cu doped SnO_2 particles as in the preparation of pure SnO_2 nanoparticles. Finally, the obtained Cu doped SnO_2 samples were used for studies.

Structure and crystalline size of the samples were determined by XRD using a PANalytical X'pert-Pro diffractometer with Cu-Kα wavelength of 1.5406 Å in 2θ range from 20° to 80°. The UV-Vis absorption spectrum was taken by Shimadzu-UV 2450 spectrophotometer. The PL measurements were carried out by Perkin Elmer-LS 45 spectrofluorometer with an excitation wavelength 300 nm. FTIR spectra of the samples were recorded using a Shimadzu-FTIR spectrometer and room temperature magnetic measurements were obtained by LAKESHORE-7410 VSM.

Results and Discussion:

Structural properties:

Figure 1. shows the powder XRD pattern for a $Sn_xCu_{1-x}O_2$ (x=0.00, 0.02, 0.03 and 0.04) nanocrystal. All the diffraction peaks can be ascribed to tetragonal rutile structure (JCPDS card No. 41-1445) without any secondary phases such as SnO and CuO. All the samples have a similar structure which implies that the Cu atoms are incorporated into SnO_2 host lattice. Lattice parameters (a and c) and particle size were measured using the rutile (110) and (101) peaks of $Sn_xCu_{1-x}O_2$ for a variety of concentrations (x). Lattice parameters and average particle size of produced samples were shown on Table. 1. Lattice parameters (a and c) gradually increase with increase in doping concentration and reaches maximum at doping level of 3% and decreased with further increase in the doping concentration. The ionic radii of O^{2-}, Sn^{4+} and Cu^{2+} are 1.40, 0.83 and 0.87 Å respectively. The radius of Cu^{2+} is higher than that of host ion (Sn^{4+}). The crystallite size was calculated by Debye-Scherrer's formula and Williamson-Hall (W-H) plot as well. Because using W-H plot the effect of strain on the crystallite size can be calculated but in Debye's method does not consider strain. The average crystallite size of sample was calculated using Debye-Scherrer's formula.

$$d = \frac{k\lambda}{\beta \cos\theta} \qquad (1)$$

Where d is the mean crystalline size, K is a grain shape factor (0.9), λ is the wavelength of the incident Cu-Kα beam, θ is a Bragg's reflection angle and β is the full width at half maximum. The following equation is applied to find the crystallite size and lattice strain of the samples by using W-H analysis.

$$\beta \cos\theta = \frac{k\lambda}{d} + 4\varepsilon \tan\theta \qquad (2)$$

The W-H plot is drawn with 4sinθ along the x-axis and βcosθ along the y-axis for as-prepared SnO_2 nanoparticles are shown in Fig.2. The crystalline size was calculated from the y-intercept of linear fit of the data, and the strain ε was measured from the slope of the linear fit. Increase in Cu concentration leads to distort

the system and it reduced the average size of the crystallite. The negative strain means contraction in the system and hence doped system has lower W-H calculated crystallite size values compared to the crystallite sizes calculated by Scherrer's equation.

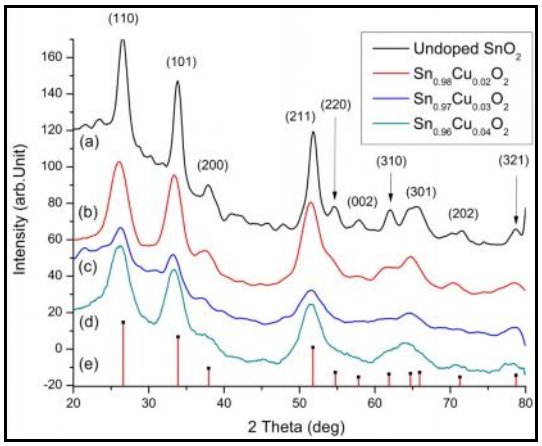

Fig. 1. XRD pattern of a) undoped SnO_2 nanoparticles, b) 2% Cu doped sample, c) 3% Cu doped sample d) 4% Cu doped sample and e) JCPDS card No: 41-1445

Table 1. Lattice parameters and average particle size of synthesized samples.

Sample	(h k l)	d-Spacing (Å)	Grain size (nm)		Lattice parameters (Å)		Lattice strain
			Scherrer's method	W-H method	a	c	
Undoped SnO_2	(110) (101)	3.35422 2.64477	10.57	26.26	4.7436	3.1859	0.0059
$Sn_{0.98}Cu_{0.02}O_2$	(110) (101)	3.42047 2.68212	4.54	35.46	4.8373	3.2229	0.0321
$Sn_{0.97}Cu_{0.03}O_2$	(110) (101)	3.45978 2.69164	3.04	0.96	4.8929	3.2232	-0.0679
$Sn_{0.96}Cu_{0.04}O_2$	(110) (101)	3.41177 2.67032	5.57	13.13	4.8250	3.2061	0.0132

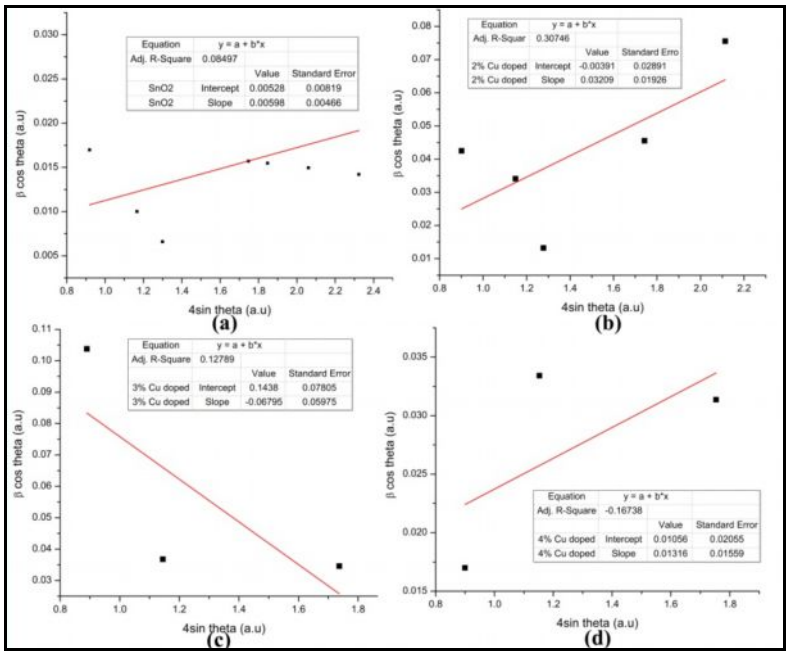

Fig. 2. W-H plot of a) undoped SnO_2 nanoparticles, b) 2% Cu doped sample, c) 3% Cu doped sample and d) 4% Cu doped sample.

Optical measurements:

FT-IR spectra of all the samples are shown in Figure.3. From the spectra we can clearly seen that changes in positions, sizes and shapes indicating that Cu have incorporated in SnO_2 host lattice. The absorption peak at 635 cm^{-1} arises from the bending vibration of Sn-O-Sn. All the samples show the broad band centered at ~3420 cm^{-1} which could be ascribed to stretching vibration of surface hydroxyl groups. It is most likely due to re-absorption water from the ambient atmosphere[25]. The peak appeared at 2920 cm^{-1} is attributed to the C-H stretching vibration[26]. This peak was decreased with increasing Cu concentration. The band appearing in all the samples around 1640 cm^{-1} may be ascribed to the bending mode O-H bonds. These results are in agreement with the earlier reports[27,28]

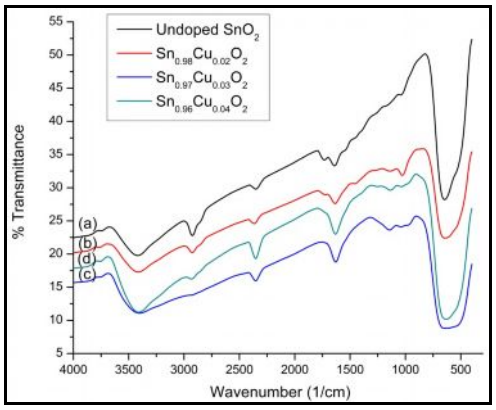

Fig. 3. FTIR spectra of a) undoped SnO_2 nanoparticles, b) 2% Cu doped sample, c) 3% Cu doped sample and d) 4% Cu doped sample.

Optical absorption measurements were carried out for to determine the optical band gap and effect of Cu incorporation replacing Sn^{4+} ions in semiconducting SnO_2 host lattice. The optical band gap values were obtained from the optical absorption spectra by using Tauc's relation.

$$\alpha h\nu = A(h\nu - E_g)^n \qquad (3)$$

Where α is the linear absorption coefficient of the sample, (hν) is the incident photon energy, A is the energy independent constant, E_g is the optical band gap energy and n is a constant which determines the type of optical transition, for direct transition, n=1/2 . Tauc's plot of all the samples was shown in figure.4. For undoped SnO_2, the calculated value of band gap is ~3.98 eV. It interesting to note that there is a red shift in band gap values of Cu doped SnO_2 samples when compared with undoped SnO_2 and a similar report was reported earlier[29]. Further, the band gap was found to increase from 3.21eV to 3.50 eV with decreasing particle size indicating that there is a blue shift in the absorption edge. This blue shift may be attributed to strong quantum confinement effect. The observed optical band gap variation might be due to changes in the band structure caused by changes in local disorder from the crystalline size of the samples and sp-d exchange interaction between the band electrons and the localized d electrons of Cu^{2+} ions substituting Sn^{4+} ions.

The PL technique has been widely used to investigate the structures and defects of metal oxides. Figure.5 shows room-temperature PL emission spectra of Cu-doped SnO_2 nanocrystal. All of the PL spectra consist of three high intensity emission peaks (at 361 nm, 377 nm and 410 nm) and one low intensity peak in the visible region (at 493 nm). This emission band contributed to twofold coordinated tin oxygen deficient centers. The PL spectra of all the samples show a strong UV emission and it is divided into two peaks. The PL intensities are initially increased with increasing Cu concentration and then decrease. The peak at 410 nm is attributed to the recombination of the deep trapped charged and photo-generated electron from the conduction band. Commonly, oxygen vacancies are known to be the most common defects in oxide based semiconductor and act as radiative centers in luminescence process. The SnO_2 nanoparticles are found to exhibit an emission peak in blue-green region centred at 493 nm. The origin of deep blue-green emission in SnO_2 nanostructures can be originated from different crystalline defects such as oxygen vacancy and Sn vacancy[30].

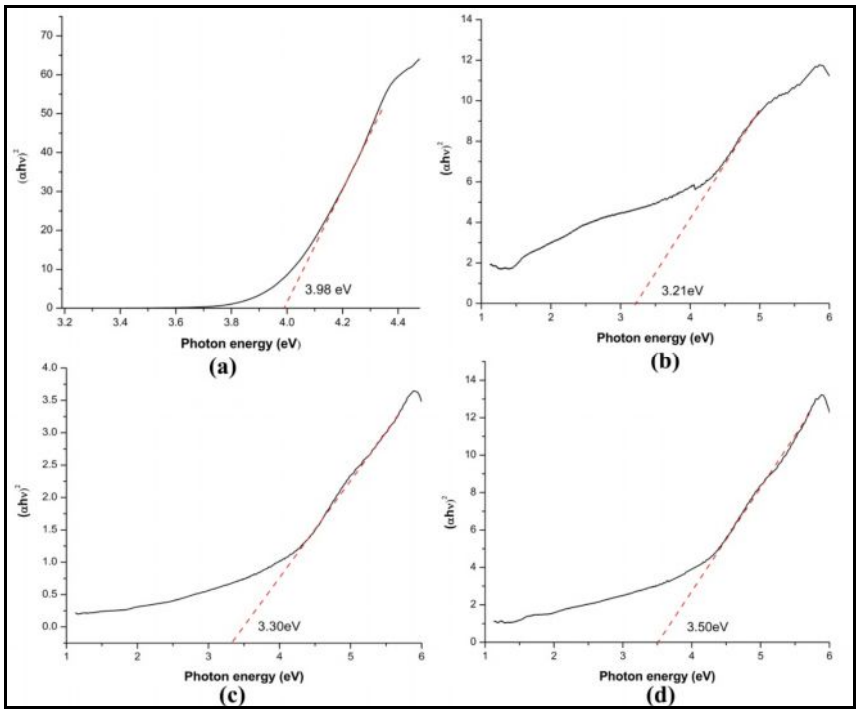

Fig. 4. Tauc's plot of a) undoped SnO_2 nanoparticles, b) 2% Cu doped sample, c) 3% Cu doped sample and d) 4% Cu doped sample.

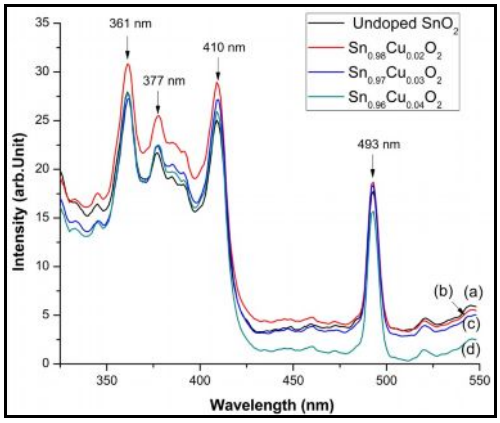

Fig. 5. Room temperature PL emission spectra of (a) undoped SnO_2 nanoparticles, (b) 2% Cu doped sample, (c) 3% Cu doped sample and (d) 4% Cu doped sample.

Magnetic studies:

For understand the magnetic behaviour of $Sn_{1-x}Cu_xO_2$ (x=0.00, 0.02, 0.03 and 0.04) nanoparticles, measurements of room temperature magnetisation as a function of magnetic field M(H) was carried out using VSM. Defects and oxygen vacancy must play important role in magnetism of these systems. Figure.6 shows the M-H behaviour of undoped and 2% Cu doped samples. Undoped sample shows perfect hysteresis loop with saturation magnetization value of 0.00776 emu\g and coercivity of 456 Oe but 2% Cu doped sample shows diamagnetic bahavior at higher values of magnetic fields. The inset of the Fig.6 shows the magnified image of 2% Cu doped sample. The origin of observed ferromagnetism whether intrinsic or due to the presence of hidden secondary phases of ferromagnetic metal cluster or their ferromagnetic oxides, regarding the exchange interactions in ferromagnetic ordering whether mediated by holes or electrons, again whether the carriers are delocalized or localized in nature. From the XRD pattern we conclude that there is no secondary phases are present in the samples. Therefore the observed ferromagnetic behaviour is due to structural defects. Defects in oxide, which trap two electrons or holes, can have a spin triplet as the ground state or as a low-lying excited state. Such centers in monoxides include the V^o cation vacancy center with two holes, and the pair of singly occupied F centers[31]. Cu^{2+} and Sn^{4+} have different valencies, which may lead to high-density doping induced defects. Cu doping has induced the expansion in SnO_2 lattice and significant structural disorder indicated by the

XRD signal broadening. Such structural changes might have destroyed the ferromagnetic ordering since the magnetic exchange interaction is sensitive to the distance between the interacting spins.

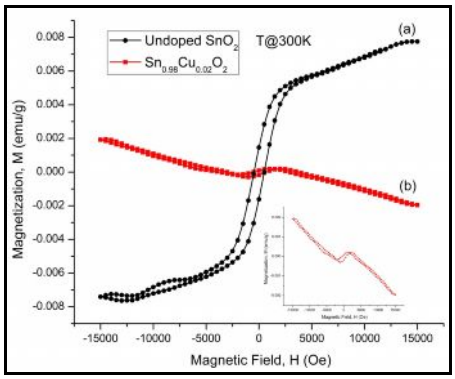

Fig. 6. M-H magnetic hysteresis loop of (a) undoped SnO_2 nanoparticles and (b) 2% Cu doped sample. Inset of the figure shows the focussed view of 2% Cu doped sample.

Conclusions:

We have successfully synthesized the Cu-doped SnO_2 nanoparticles by a sol-gel method. It is observed from the XRD study that the prepared samples with Cu-doping percentage varying from 2 to 4% shows a SnO_2 rutile phase and the lattice parameters are increased with increasing Cu concentration only up to 3% while it is decreased beyond 3 %. From the FTIR spectra, we can see that the peak changes are in accordance with the incorporation of Cu^{2+} ions into the SnO_2 lattice. Band gap values of 2-4% Cu doped samples vary from 3.21 to 3.50 eV, which ensures that the optical properties change with respect to the quantum confinement effect in nanocrystal. The PL intensities increase with increasing Cu concentration. The maximum luminescence is observed for 2% Cu doped sample. The room temperature ferromagnetism of undoped SnO_2 sample is activated by the structural disorder like oxygen vacancy, where as Cu doped sample shows the diamagnetic property at higher fields. The diamagnetic property on doping may be due to the structural disorder, electronic structural modifications and surface nature of the nanocrystallites. The present work provides useful information for tuning the optical and structural properties of Cu- doped SnO_2 based DMS materials.

References:

1. Duan Y., Fu N., Liu Q., Fang Y., Zhou X., Zhang J. and Lin Y., Sn-Doped TiO2 Photo anode for Dye-Sensitized Solar Cells, J. Phys. Chem. C 2012, 116, 8888−8893.
2. Anshu Singhal, Achary S. N., Manjanna J., Jayakumar O. D., Kadam R. M. and Tyagi A. K., Colloidal Fe-Doped Indium Oxide Nanoparticles: Facile Synthesis, Structural, and Magnetic Properties, J. Phys. Chem. C 2009, 113, 3600–3606
3. Xiaohu Huang, Guanghai Li, Bingqiang Cao, Ming Wang and Changyi Hao, Morphology Evolution and CL Property of Ni-Doped Zinc Oxide Nanostructures with Room-Temperature Ferromagnetism, J. Phys. Chem. C 2009, 113, 4381–4385
4. Gao-Ren Li, Dun-Lin Qu, Laurent Arurault and Ye-Xiang Tong, Hierarchically Porous Gd^{3+} Doped CeO_2 Nanostructures for the Remarkable Enhancement of Optical and Magnetic Properties, The Journal of Physical Chemistry C, 113, 1235-1241.
5. Cho J. H., Hwang T. J., Joh Y. G., Kim E. C. and Dong Ho Kima, Room-temperature ferromagnetism in highly-resistive Ni-doped TiO_2, Appl. Phys. Lett., 2006, 88, 092505.
6. Nehru L.C., Swaminathan V. and Sanjeeviraja C., Photoluminescence Studies on Nanocrystalline Tin Oxide Powder for Optoelectronic Devices, American Journal of Materials Science 2012, 2, 6-10.
7. Evan T. Salem, Tin Oxide Nanoparticles Prepared Using Liquid Phase Laser Ablation for Optoelectronic Application, Nanosci. Nanotechnol., 2012, 2, 86-89.
8. Pouretedal H.R., Shafeie A. and Keshavarz M.H., Preparation, Characterization and Catalytic Activity of Tin Dioxide, J. Korean Chem. Soc. 2012, 56, 484-490.
9. Kamble V.B. and Umarji A.M., Correlating defect induced ferromagnetism and gas sensing properties of undoped tin oxide gas sensors, Appl. Phys. Lett. 2014, 104, 251912.
10. Yan-La Nuli, Sheng-Li Zhao, Qi-Zong Qin, Nanocrystalline tin oxides and nickel oxide film anodes for Li-ion batteries, J. Power Sources, 2003, 114, 113-120.

11. Gubbala S., Russell H.B., Shah H., Biswapriya-Deb, Jasinski J., Rypkemac H., Sunkara M.K., Surface properties of SnO_2 nanowires for enhanced performance with dye sensitized solar cells, Energy Environ. Sci. 2009, 2, 1302-1309.
12. Sharma A., Kumar S., Kumar R., Varshney M. and Verma K.D., Magnetic properties of Fe and Ni doped SnO_2 nanoparticles, Optoelectron. Adv. Mater., Rapid Commun. 2009, 3, 1285.
13. Gu F., Wang S.F., Lu M.K., Qi Y.X., Zhou G.J., Xu D. and Yuan D.R., Luminescent characteristics of Eu^{3+} in SnO2 nanoparticles, Opt. Mater. 2004, 25, 59-64.
14. Nakano Y., Morikawa T., Ohwaki T. and Taga Y., Band-gap narrowing of TiO_2 films induced by N-doping, Physica B 2006, 376, 823-826.
15. Li Y.R., Liang Z., Zhang Y., Zhu J., Jiang S.W. and Wei X.H. Growth modes transition induced by strain relaxation in epitaxial MgO thin films on $SrTiO_3$ (001) substrates, Thin Solid Films, 2005, 483, 245-250.
16. Kwak J. K., Park K.H., Yun D.Y., Lee D. and Kim T. W., Microstrucural and Optical Properties of SnO_2 Nanoparticles Formed by Using a Solvothermal Synthesis Method, J. Korean Phys. Soc., 2010, 57, 1803-1806.
17. Yue Li, YanqunGuo, Ruiqin Tan, Ping Cui, Yong Li, Weijie Song , Synthesis of SnO_2 nano-sheets by a template-free hydrothermal method, Mater. Lett. 2009, 63, 2085-2088.
18. Bernardi M.I.B., Feitosa C.A.C., Paskocimas C.A., Longo E. and Paiva-Santos C.O., Development of metal oxide nanoparticles by soft chemical method, Ceram. Int. 209, 35, 463-466.
19. Yang H., Hu Y., Tang A., Jin S., Qiu G., Synthesis of tin oxide nanoparticles by mechanochemical reaction, J. Alloys Compd. 2004, 363, 276-279.
20. Yanhui C., Xingtang Z., Zhonghui X., Yuncai L., Yabin H., Zuliang D. and Tiejin L., Fabrication and structural characterization of large-scale uniform SnO_2 nanotube arrays by sol-gel method, Chin. Sci. Bull. 2005, 50, 618-621.
21. Liu B., Cheng C.W., Chen R., Shen Z.X., Fan H.J., Sun H.D., Fine Structure of Ultraviolet Photoluminescence of Tin Oxide Nanowires, J. Phys. Chem. C 2010, 114, 3407-3410.
22. Arai T. and Adachi S., IR Emission Band and Multiple-Peak Structure in Photoluminescence Spectra of SnO_2:Mn , ECS J. Solid State Sci. Technol. 2013, 2, 172-177.
23. Shao-Bo H., Shi-Fa W., Qing-Ping D., Xiao-Dong Y., Wan-Guo Z., Xia X., Zhi-Jie L. and Xiao-Tao Z., Role of chelating agent in chemical and fluorescent properties of SnO_2 nanoparticles, Chin. Phys. B 2013, 22, 058102.
24. Singh A.K. and Nakate U. T., Microwave Synthesis, Characterization and Photocatalytic Properties of SnO2 Nanoparticles, Adv. Nanopart. 2013, 2, 66-70.
25. S.H. Luo, P.K. Chu, Z.F. Di, M. Zhang, W.L. Liu, C.L. Lin, J.Y. Fan, X.L. Wu, Vacuum electron field emission from SnO_2 nanowhiskers annealed in N_2 and O_2 atmospheres, Appl. Phys. Lett. 2006, 88, 013109.
26. Y.H. Ao, J.J. Xu, D.G. Fu, Study on the effect of different acids on the structure and photocatalytic activity of mesoporous titania, Appl. Surf. Sci. 2009, 256, 239–245.
27. He Jianga, Xiao Fang Liub, Zhi Yu Zoub, Zhang Ben Wua, Bo Hec, Rong Hai Yub, The effect of surfactants on the magnetic and optical properties of Co-doped SnO_2 nanoparticles, Appl. Surf. Sci., 2011, 258, 236– 241
28. Srinivas K., Vithal M., Sreedhar B., Manivel Raja M., and Venugopal Reddy P., Structural, Optical, and Magnetic Properties of Nanocrystalline Co Doped SnO_2 Based Diluted Magnetic Semiconductors, J. Phys. Chem. C 2009, 113, 3543–3552
29. Bouaine A., Brihi N., Schmerber G., Ulhaq-Bouillet C., Colis S. and Dinia A. Structural, Optical, and Magnetic Properties of Co-doped SnO_2 Powders Synthesized by the Coprecipitation Technique, J. Phys. Chem. C 2007, 111, 2924-2928.
30. He H., Wu T.H., Hsin C.L., Li K.M., Chen L.J., Chueh Y.L., Chou L.J. and Wang Z.L., Beaklike SnO2 nanorods with strong photoluminescent and field-emission properties, Small, 2006, 2, 116-120.
31. Stoneham A. M., Theory of Defects in Solids, Chap. 16, Clarendon Press, Oxford, 1975.

*****